Assessment of overlay masonry strengthening system under in-plane monotonic and cyclic loading using the diagonal tensile test

João A. P.P. Almeida[1], Eduardo B. Pereira[2], Joaquim A. O. Barros[3]

ISISE, University of Minho, Department of Civil Engineering, School of Engineering, Azurém, 4810-058 Guimarães, Portugal

ABSTRACT

The development of novel strengthening techniques to address the seismic vulnerability of masonry elements is gradually leading to simpler, faster and more effective strengthening strategies. In particular, the use of fabric reinforced cementitious matrix systems is considered of great potential, given the increase of ductility achieved with simple and economic strengthening procedures. To assess the effectiveness of these strengthening systems, and considering that the seismic action is involved, one important component of the structural behaviour is the in-plane cyclic response. In this work is discussed the applicability of the diagonal tensile test for the assessment of the cyclic response of strengthened masonry. The results obtained allowed to assess the contribution of the strengthening system to the increase of the load carrying capacity of masonry elements, as well as to evaluate the damage evolution and the stiffness degradation mechanisms developing under cyclic loading.

---

[1] PhD candidate, ISISE, Dep. of Civil Engineering, University of Minho, Campos de Azurém, 4800-058 Guimarães, Portugal. Phone: +351 253 510 215, E-mail: japp.almeida@gmail.com (corresponding author)

[2] Assistant Professor, ISISE, Dep. of Civil Engineering, University of Minho, Campos de Azurém, 4800-058 Guimarães, Portugal. Phone: +351 253 510 487, E-mail: epereira@civil.uminho.pt

[3] Professor, ISISE, Dep. of Civil Engineering, University of Minho, Campos de Azurém, 4800-058 Guimarães, Portugal. Phone: +351 253 510 210, E-mail: barros@civil.uminho.pt

Keywords: infill masonry, high ductility, strengthening system, shear capacity, in-plane cyclic tests, experimental characterization

HIGHLIGHTS

- The efficiency of FRCM overlays was assessed as part of a masonry strengthening system.
- The strength increment of masonry walls was quantified by diagonal tensile tests.
- Monotonic and cyclic in-plane loading was applied to evaluate the behaviour of the walls.
- The key failure modes obtained experimentally and the basic mechanisms were examined.
- Experimental results were discussed and compared to the analytical model predictions.

Nomenclature:

FRCM	Fabric reinforced cementitious matrix
A_f	Area of the mesh reinforcement by unit width
A_m	Interface loading area between the steel shoe and the specimen
A_n	Net area of the specimen cross section
$A_{n,r}$	Net area of the render cross section
$A_{n,PFRM}$	Net area of the PFRM cross section
E_f	Tensile modulus of elasticity of the cracked FRCM specimen
f_{fv}	Design tensile strength of FRCM reinforcement
$f_{fv,ult}$	Ultimate tensile strength of FRCM reinforcement
f'_m	Compressive strength of the masonry
f'_t	Tensile strength of the masonry
g	Vertical gage length
G	Modulus of stiffness in shear
h	Height of the brick units
L	Length of the wall in the direction of the shear force
n	Number of fabric layers
n^*	Percentage of the net area
P	Applied load
S_s	Shear stress
t	Thickness of the specimen
V_{ref}^{exp}	Shear capacity of the reference specimens obtained experimentally
V_{str}^{exp}	Shear capacity of the strengthened specimens obtained experimentally
V_{ACI}^{an}	Shear capacity of the specimen calculated following the ACI549.4R-13
$V_{ACI+PFRM}^{an}$	Shear capacity of the specimen calculated following ACI549.4R-13 plus the contribution of the PFRM layers

V_{Sup}^{an}	Shear capacity of the specimen considering ultimate strain of the FRCM plus the contribution of the PFRM layers
V_{dt}	Shear capacity due to diagonal tension failure
V_f	Shear capacity of the FRCM system
V_m	Shear capacity of the masonry specimen
V_{sf}	Shear capacity due to shear friction failure
V_{ss}	Shear capacity due to shear sliding failure
$V_{f,ult}$	Shear capacity of the FRCM system considering ultimate tensile strain
V_r	Shear capacity of the render layer
V_{PFRM}	Shear capacity of the PFRM layer
u_v	Vertical shortening
u_h	Horizontal elongation
w	Length of brick units
γ	Shearing strain
ε_{fv}	Design value of the tensile strain of FRCM reinforcement
$\varepsilon_{fv,ult}$	Tensile strain ultimate value of FRCM reinforcement
μ_0	Coefficient of internal shear friction in mortar joint
μ_m	Modified coefficient of internal shear friction in mortar joint
τ_0	Shear bond strength of the mortar joint
$\tau_{0,m}$	Modified shear bond strength of the mortar joint
θ	Angle between horizontal and main diagonal of the wall

1. INTRODUCTION

Masonry constructions are composed of brittle or quasi-brittle materials, and generally have low resistance to seismic events. The current performance requirements prescribed by the design codes are frequently not accomplished by existing constructions, either because these requirements became more demanding, or because the negative effects of aging in the long-term behaviour of the materials resulted in a substantial decrease of the load carrying capacity of the masonry elements. Therefore, the development of effective procedures to retrofit existing masonry constructions, in order to upgrade their load bearing capacity and increase their ductility response, is still of great importance.

This work presents the experimental program developed with the aim of characterizing and quantifying the contribution of a strengthening system based on fabric reinforced cementitious matrix (FRCM) to the increase of the load carrying capacity and deformability of masonry elements subjected to in-plane loading. In addition, this research investigates the adequacy and effectiveness of the application of the diagonal tensile test for the evaluation of the in-plane cyclic behaviour of strengthened masonry elements. The test procedure, which will be detailed in the following sections, was adapted in order to consider unidirectional cycles of loading and unloading.

1.1. Overlay strengthening techniques

The application of additional overlays to the existing masonry elements is a common strengthening technique, especially in areas of considerable seismic activity. Generally, the strengthening overlay consists of a mortar, applied manually or mechanically. These surface treatments, as designated by Elgaway et al., [1], typically incorporate different types of steel, polymers, carbon or glass fibres and fibre meshes used to enhance tensile behaviour and ductility of the strengthening overlay, [2-6]. The application of these reinforced strengthening overlays improves both the in-plane and the out-of-plane load carrying capacity, [7]. A different concept of overlay strengthening system was developed by using materials with tensile strain-hardening behaviour in the hardened state, avoiding the use of reinforcement meshes. These materials, with the designation of strain hardening cement composites (SHCC), have a tensile strength higher than the stress at crack initiation, and a tensile strain at tensile strength higher than 1%, with the capacity of developing diffuse crack patterns of a maximum crack width does not exceeding 0.1 mm in the hardening phase. The SHCC can be applied using the shotcreting technique or manually, [8-9]. This technique can lead to the increase of the shear capacity of the masonry, to the improvement of its deformability and to the enhancement of its energy dissipation capacity during cyclic loading, [10].

Some of the advantages and disadvantages of the masonry strengthening techniques based on the addition of strengthening overlays to the original masonry element are presented by Elgaway et al, [1], [11]. The advantages identified include the low cost, the durability, the uniform behaviour, the increase of in-plane strength up to 3.6 times, the improvement of the out-of-plane stability and the increase of the energy dissipation ability before failure. The increase of the dead weight of the strengthened elements, the requirement of surface treatments, the architectural changes of the structure, and the high disturbance during works are the main disadvantages identified, [1], [11]. The increase of the stiffness in shear walls due to the application of thick strengthening overlays may also lead to alterations of the structural behaviour. These alterations often result in substantial increments of the stresses at these elements, which in turn may lead to the increase of their strength requirements. In addition, the greater stiffness of the strengthening overlays, when compared to the original substrates, is especially demanding at the level of the interface, where high stresses are generated and the delamination of the overlay is promoted.

1.2. In-plane experimental characterization

The characterization of the structural behaviour of masonry elements is typically divided in two main different types, depending on the loading configuration: the in-plane and the out-of-plane behaviours, [12-13]. Concerning the in-plane characterization, the monotonic shear behaviour of elements is often assessed by means of the diagonal tensile tests, using masonry specimens built in the laboratory, [14-15], or in-situ [16-17]. Different types of strengthening systems have already been evaluated using this type of test, [10], [17-20]. As discussed in previous publications, Almeida et al. [21] the cyclic shear behaviour of masonry panels can be characterized by means of the diagonal tensile test. Brignola et al [16] conducted force controlled cyclic tests, with a load gradient of 200 N/s, and the loading procedure was defined in order to obtain four or five cyclic load steps for each masonry panel. In the experimental campaign presented by Santa-Maria et al [22], the test procedure started with the first diagonal loading and unloading, followed by the loading of the second diagonal and unloading. Two cycles were performed at each load level, the load increments at each level were of 25 kN.

The diagonal tensile test is regarded as a simple and expedite procedure for the in-plane behaviour characterization. However, it is important to stress that the capability of this type of test to disclose all the failure modes of masonry walls is limited. For example, the rocking/crushing mechanism cannot be evaluated, [17]. For the evaluation of those mechanisms, other experimental procedures, such as the one used by Pinho et al, [23], or Vasconcelos et al, [24] must be carried out.

A summary of data available in literature referred to diagonal tensile tests on unreinforced clay brick masonry strengthened with additional overlays or composite materials is presented in Table 1. Different types of masonry and strengthening systems are presented. It is possible to verify that most of the authors use a reduced amount of specimens for the characterization of a specific layout. However, whenever possible the coefficient of variation was calculated and the results obtained are in general quite low, especially for strengthened panels. Therefore the use of a reduced number of specimens seems to lead to sufficiently representative experimental results.

Table 1 - Summary of previous diagonal tensile test results on strengthened URM specimens.

Reference	Type of masonry	Dimension of blockst (mm)	Dimension of the panel (mm) *h*	*l*	*t*	Nº of panels	Type of reinforcement	F_{max} (kN)	S_s (MPa)	CoV (%)	Capacity increment (%)
Santa-Maria et al. [22]	HCBM	290x140x112	1060	1100	140	5	--	132	--	15	--
						4	2 diagonal 150 mm-wide CFRP laminate	226	--	2	71
						5	2 diagonal CFRP fabric	196	--	4	48
						4	2 horizontal 150 mm-wide CFRP laminate	144	--	6	9
						5	2 horizontal CFRP fabric	182	--	8	38
Gabor et al. [25]	HCBM+CM	210x100x50	870	840	100	2	--	234	--	--	--
						1	unidirectional glass fibre, RFV	332	--	--	42
						1	unidirectional carbon fibre, RFC	361	--	--	54
						1	bidirectional glass fibre, RFW	384	--	--	64
Ozsayin et al. [26]	PCBM +CLM	87x84x56	350	350	70	2	--	--	0.95	--	--
						2	CFRP, strips	--	1.98	--	108
						2	CFRP, full surface	--	2.25	--	137
	PCBM +CM		500	500	70	2	--	--	0.92	--	--
						2	CFRP, strips	--	1.29	--	40
						2	CFRP, full surface	--	2.38	--	159
	PCBM +CLM					2	--	--	0.6	--	--
						2	CFRP, strips	--	1.39	--	132
						2	CFRP, full surface	--	1.16	--	93
Kadam et al. [2]	SCBM one-wythe thick+CM	230x110x70	700	700	110	3	--	25	--	2	--
					160	3	unidirectionally anchored welded wire mesh	164	--	7	561
						3	bidirectionally anchored welded wire mesh	174	--	13	602
	SCBM two-wythe thick+CM		750	750	230	3	--	46	--	7	--
					280	3	unidirectionally anchored welded wire mesh	236	--	8	413
						3	bidirectionally anchored welded wire mesh	223	--	15	385
Dehghani et al. [10]	SCBM+CM	225x105x40	450	450	105	2	--	51	--	--	
						8	ECC, (ft=3.8; fc=47 MPa), LT:10 and 15 mm	70-142	--	--	37-178

Where: PCBM= perforated clay brick masonry; HCBM= hollow clay brick masonry; SCBM= solid clay brick masonry; CM= cement mortar; CLM= cement and lime mortar; LT= layer thickness.

The test setup adopted for the diagonal tensile tests is represented in Figure 1 and complies with the experimental procedure described by ASTM-E519-02, [12]. The dimensions of the panels were set to 0.99x0.99 m considering equipment constrains, symmetry conditions and the dimensions adopted by other authors using similar brick dimensions and panel configurations. As discussed by Brignola et al. [16] and Calderini et al., [27], and evaluated by Frocht [28] the elastic solution considering homogeneous isotropic continuum providing the following stress state at the centre of the panel when only a diagonal compressive load is applied, $q = 0$: $\sigma_x = \sigma_y \cong -0.56P/A$; $\tau_{xy} = 1.05P/A$; $\sigma_I \cong 0.5P/A$; $\sigma_{II} \cong -1.62P/A$. Where A is the transversal area of the panel, P is assumed as positive and the loading direction angle always being 45º. The Mohr´s representation of the stress state in this region is depicted in Figure 2.

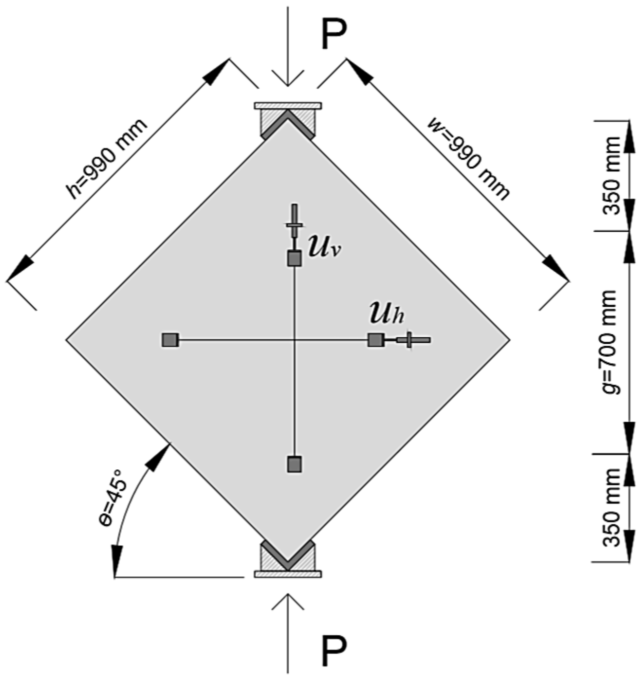

Figure 1 – Diagonal tensile test: a) general set-up

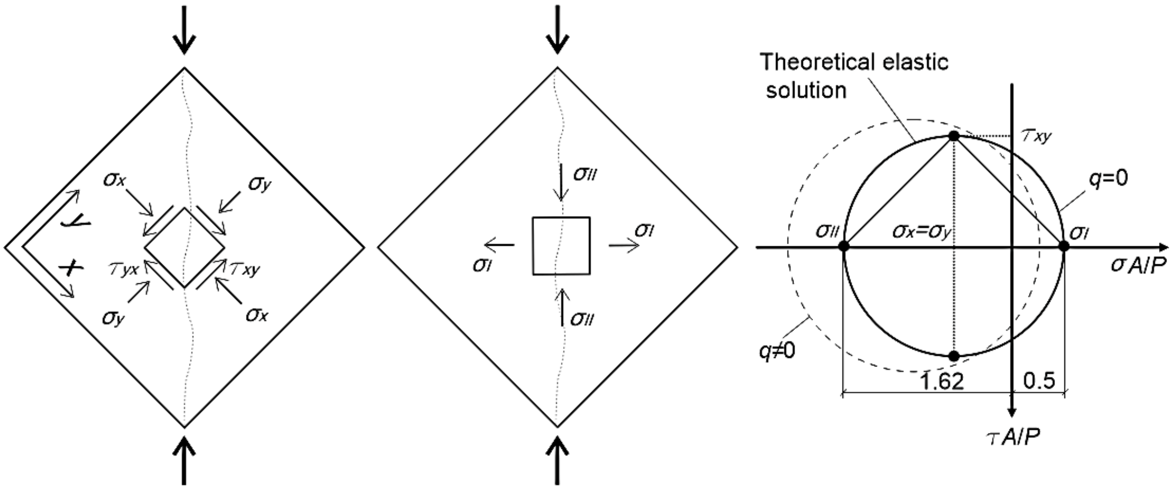

Figure 2 – Mohr's representation of the stress state assumed in the central area of the specimen.

The values of the shear stress, shear strain and modulus of shear stiffness in the centre of the panel are also obtained according the procedures indicated in ASTM-E519-02, [12], in this case the stress state is characterized by a $\tau_{xy} = \sigma_I = \sigma_{II}$, [16]. The shear stress is obtained by the equation (1):

$$S_s = \frac{0.707 \times P}{A_n} \qquad (1)$$

where P is the applied load, A_n is the net area of the specimen's cross-section calculated according to equation (2):

$$A_n = \left(\frac{w+h}{2}\right) \times t \times n^* \qquad (2)$$

where w, h and t are, respectively, the width, the height, and the total thickness of the specimen, and n^* is the percentage of the gross area of the unit that is solid, expressed as a decimal.

The shear strain is computed as shown in equation (3):

$$\gamma = \frac{u_v + u_h}{g} \qquad (3)$$

where γ is the shearing strain, u_v is the vertical shortening, u_h is the horizontal elongation and g is the vertical gage length.

Finally, the modulus of stiffness in shear is calculated as shown in equation (4):

$$G = \frac{S_s}{\gamma} \qquad (4)$$

2. OBJECTIVES AND RESEARCH SIGNIFICANCE

This research discusses the relevance of diagonal tensile test for the characterization of the "in-plane" monotonic and cyclic behaviour of masonry specimens. An expeditious procedure is developed and applied to quantify the contribution of the reinforcement system to improve the masonry behaviour. The identification and interpretation of the damage mechanisms that develop during the diagonal tensile tests are presented, and an extrapolation of these to practical situations is discussed. Finally, a review of analytical calculation procedures to estimate the load carrying capacity and identify the mechanisms leading to rupture of strengthened masonry is carried out, and the results are presented and discussed.

3. MATERIALS AND METHODS

3.1. Materials used in the experiments

The materials used in the preparation of the masonry elements, representative of infill walls, and of the strengthening system were selected with the intention of representing regional real cases as much as possible. Although lime mortars are also frequently used in the structural rehabilitation of masonry walls, the system investigated was only based on Portland cement as binder. The masonry specimens were assembled using ceramic bricks (Length x Height x Thickness: 28.5x19.5x11.0 cm^3) and the following cement mortar for the joints: Portland cement 32.5N, medium graded river sand and water, in a volume ratio of 1:5:2. After a layer of roughcast was applied: Portland cement 32.5N, medium graded river sand and water, in a volume ratio of 1:4:2. Finally a render layer of a cementitious mortar with a thickness of 1.5 cm was added on both faces of the masonry specimen, same composition as the mortar used in the joints. The composition and workability of the mortars were initially optimized, and then remained similar for all the assembled specimens. The main mechanical properties of the used materials were experimentally assessed, and the results obtained are summarized in Table 2.

Table 2 – Properties of the masonry components

Masonry components	
Compressive strength of units, parallel to hollows, EN 772-1 [29] *,**	6.55 (8%) N/mm^2
Compressive strength of units, normal to hollows, EN 772-1 [29] *,**	2.21 (9%) N/mm^2
Compressive strength, mortar joints and render, EN 1015-11 [30] *	8.58 (7%) N/mm^2
Flexural strength, mortar joints and render, EN 1015-11 [30] *	2.11 (3%) N/mm^2
Adhesion strength to render layer to brick, EN 1015-12 [31] *	0.51 (22%) N/mm^2

*The values in parenthesis represent the coefficient of variation.
**Values obtained experimentally in dry air condition state.

A commercially available system, herein designated FRMCom, was used for the strengthening of the masonry specimens. The FRMCom combines a carbon fibre mesh (CFM) with a cementitious mortar matrix reinforced with polypropylene fibres (PFRM). The polypropylene fibres have the main function of preventing cracking shrinkage of the mortar, while the CFM aims to assure strengthening attributes to the FRMCom system. The experimental results obtained from the characterization of the main physical and mechanical properties of the PFRM in the hardened state are summarized in Table 3, and the corresponding followed standards are indicated. The mechanical tests were conducted in all cases 28 days after casting, in agreement with the EN 1015-11, [30]. The flexural strength was obtained by averaging the results obtained in 3 specimens and the compressive strength was obtained by averaging the results obtained in 6 specimens. All specimens were cured in laboratory ambient conditions, at an average temperature of 19+/-2ºC and a relative humidity of about 55% +/- 10%. The bending tests were performed by applying a constant load increment of 35 N/s and the compression tests were executed by applying an increasing force at a constant loading rate of 400 N/s until failure.

Table 3 – Properties of the *PFRM*

PFRM	
Density	2050 kg/m^3
Amount of water	14% by weight
Elasticity Modulus, [32]	40000 N/mm^2
Compressive strength*, EN 1015-11 [30]	44 (6%) N/mm^2
Flexural strength*, EN 1015-11 [30]	3.27 (6%) N/mm^2
Adhesion strength to render layer*, EN 1015-12 [31]	1.48 (20%) N/mm^2

* Values in parenthesis represent the coefficient of variation.

The adhesion strength was evaluated by means of pull-off tests conducted according the EN 1015-12, [31]. The specimens with 30x20x13.5 cm^3 were built following the same process used for the specimens of diagonal tensile tests and cured at constant temperature and relative humidity of 20ºC and 90%, respectively, [31]. The preparation of the samples for testing implied the execution of a circular slot with a depth of 27 mm and a diameter of 50 mm, using a core drilling machine and water for easier cutting and for avoiding excessive vibrations. After cleaning the surface, a metallic plate was bonded to the test area. The metallic plate was later attached to the pull-off machine, after the initial levelling of the equipment, an increasing traction force was applied at a constant loading rate of 40 N/s. The maximum force recorded corresponds to the adhesion force that after has been divided by the area of the core providing the adhesion strength. The pull-off tests were carried out 28 days after casting.

In Table 4 the properties of the CFM are presented, according to the data provided by the supplier, [32].

Table 4 – Properties of the *CFM,* [32]

CFM	
Carbon fibres in both directions	50 threads/m
Elastic modulus	≥240 kN/mm^2
Tensile strength	≥4300 N/mm^2
Elongation at rupture	1.75 %
Ultimate tensile force	185 kN/m

3.2. Preparation of the specimens for the diagonal tensile tests

The procedure adopted in the production of the masonry walls involved the following steps: soaking of the bricks until saturation; placement of guides to keep a constant joint thickness of 1.5 cm; levelling of the bedding mortar; placement and levelling of a row of bricks; placement of vertical mortar joints with a thickness of 1.5 cm; verification of the thickness of the joints; check the plumb; repeat the previous steps until the wall was finished. Six walls were produced for the diagonal tensile tests, three for reference specimens and three for subsequent strengthening.

All masonry specimens (a) were sprinkled with a cement mortar (1:4:2) two days after (b), then a cement mortar layer with a thickness of 1.5 cm (volume ratio 1:5:2) was applied on both faces (c), as shown in Figure 3a) and 3b).

The specimens were strengthened using the FRMCom system, as shown in Figure 3a) and 3b), by carrying out the following steps: initial spraying of the wall with water; application of the first layer of PFRM with an approximate thickness of 1.2 cm (d); placement of the CFM on top of the PFRM layer (e); application of the second layer of PFRM with an approximate thickness of 1.2 cm (f); use of a ruler and a trowel to level and smoothen the mortar layer surfaces; spraying of the wall surfaces with water 15 min after finished, to avoid shrinkage. The strengthening operations were performed 14 days after the application of the render layer (c).

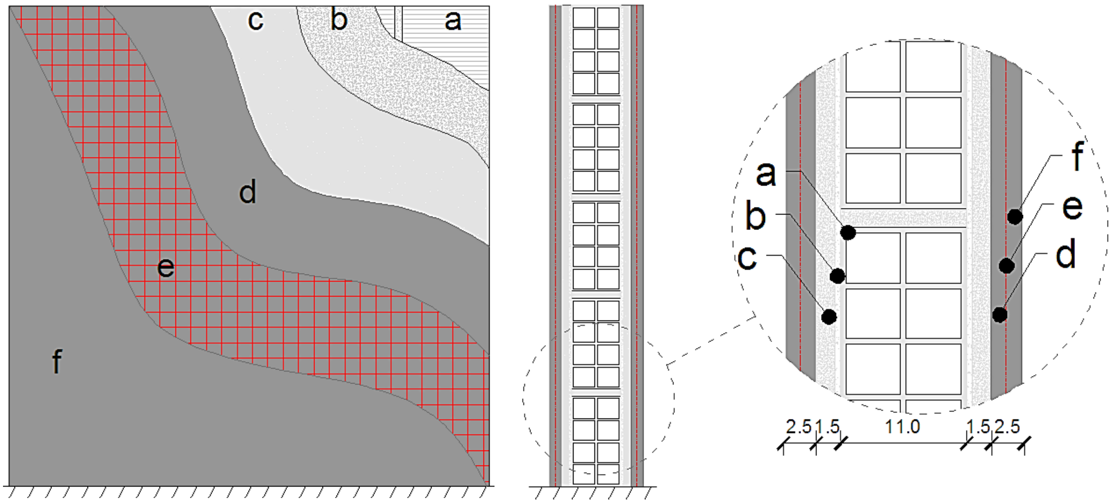

a) b)

Figure 3 - General layout of specimens: a) Procedure adopted in the production of the specimens; b) Section of the specimens and detail of the FRMCom system. (Legend: a - masonry; b - roughcast mortar, mortar 1:4:2; c - render layer 1.5 cm thick, mortar 1:5:2; d - PFRM 1.2 cm; e - CFM; f - PFRM 1.2 cm. Dimensions in cm)

3.3. Set up used for the diagonal tensile tests

Diagonal tensile tests were performed to assess the contribution of the strengthening system for increasing the load carrying capacity, the deformability and the energy dissipation performance before failure of the masonry elements when subjected to a loading scheme that resembles the in-plane shear loading conditions. The specimens had a square geometry with approximately 990 mm side, as shown in Figure 4. The number of clay blocks used in the vertical and horizontal directions was 5 and 3.3, and the symmetry of blocks and joints both in the horizontal and in the vertical directions was guaranteed. The thickness of the reference specimens was 140 mm and the thickness of the strengthened specimens was 190 mm, as shown in Figure 3.

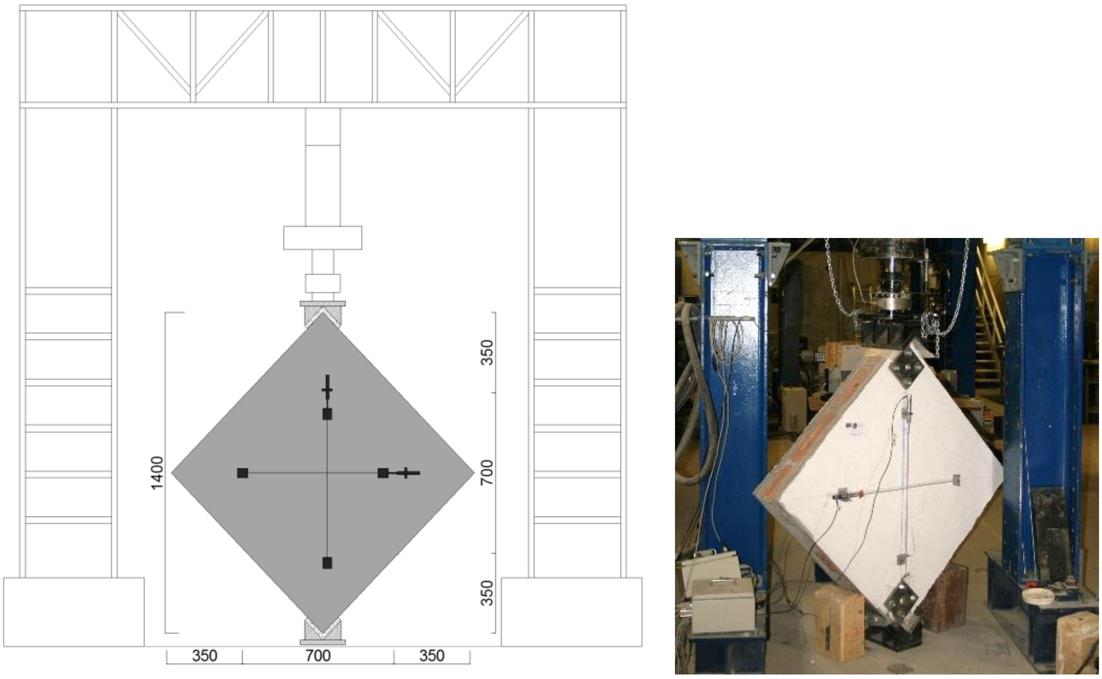

a) b)

Figure 4 - Test set-up of the direct tensile test: a) Geometry of specimens and position of LVDTs (dimensions in mm); b) Detail of the positioning of the specimen and of the test set-up.

The set-up included a testing frame, an actuator with a 500kN load cell, and a servo-hydraulic closed loop controlled system, a data acquisition system and a monitoring system composed by 5 linear variable displacement transducers (LVDT's). The vertical and horizontal deformability of both specimen surfaces were determined in the central area, between ¼ and ¾ of the diagonal of the specimen, by using 2 LVDT's in each direction, as shown in Figure 4a).

The dimensions of the steel shoes adopted a "V" shape with 152 mm in each side and 320 mm long, according to ASTM E-519-2, [12]. In the case of the strengthened specimens, the local crushing and splitting of the external strengthening layer at both loading edges were observed, as observed for specimen FRMCom_01 subsequently described. In order to avoid this premature local failure mechanism, in the subsequent specimens two steel plates were placed near the supports (150x150x30 mm^3) to provide additional confinement to the material in this region. These plates were transversely connected with 16 mm diameter steel rods crossing the specimen between the opposite faces in each support, as shown in Figure 4b).

Each test was performed using displacement control of the actuator cross-head, by measuring the displacement of the cross-head with an external LVDT. The applied displacement rate was kept constant at 0.01 mm/s, for both monotonic and cyclic tests. In the case of the cyclic tests, the displacement amplitude was gradually increased until the last cycle was reached. The amplitude of the cycles was specified considering the displacement of the actuator cross-head at the peak of the monotonic test, the increase in each cycle was determined as 1/5 of that value. A maximum number of 7 cycles were imposed, and an additional final loading cycle was imposed by applying a monotonically increasing displacement until failure was reached (Figure 5). In the case of the strengthened specimens, the experimental procedure was interrupted after the 7th cycle, due to the loss of contact between the actuator and the loading shoe. The 8th cycle was started after correcting this residual vertical deformation, by lowering 5 mm the reference initial position of the actuator cross-head, as shown in Figure 5.

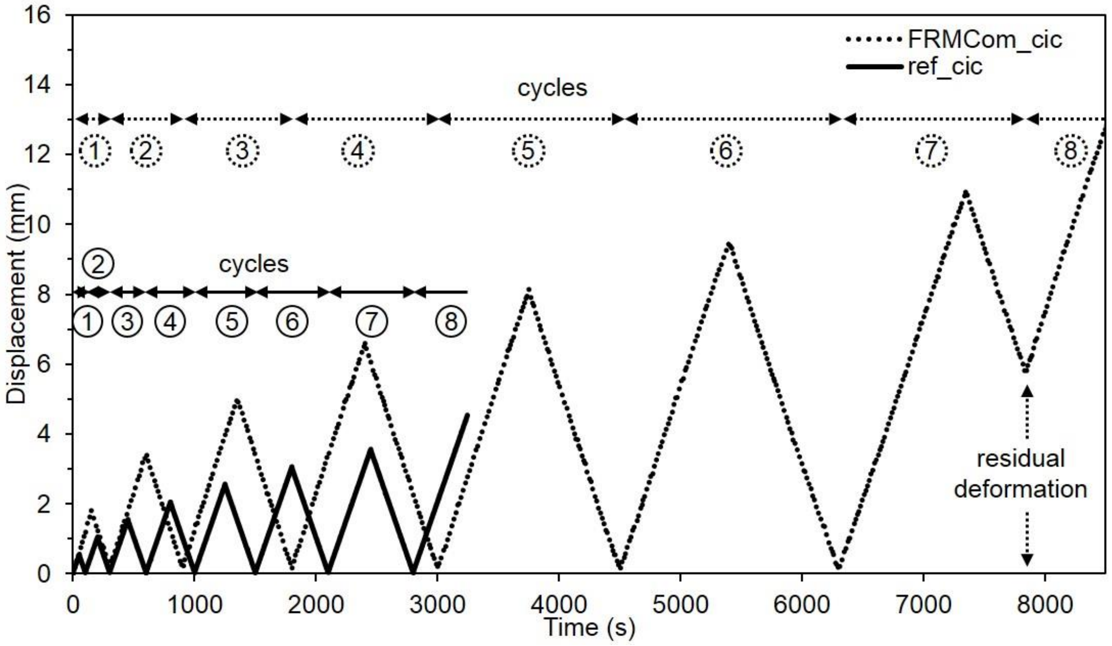

Figure 5 - Displacement laws imposed during the cyclic tests.

4. DIAGONAL TENSILE TEST RESULTS

The main results obtained for the monotonic diagonal tensile tests, which include the peak load and the corresponding horizontal and vertical average displacements, are presented in Table 5. The results obtained for the cyclic tests are presented in Table 6. For each cycle the peak load and the corresponding displacements, horizontal and vertical, are indicated in this table. For the specimens ref_03 and FRMCom_03 only the results up to the 6th and 7th cycles, respectively, are presented due to the occurrence of their premature failure at the referred cycles.

Table 5 – Monotonic diagonal tensile test results.

ref_02			FRMCom_01		
Load (kN)	u_h (mm)	u_v (mm)	Load (kN)	u_h (mm)	u_v (mm)
97.34	0.12	-0.26	409.54	1.47	-0.68

Table 6 – Cyclic diagonal compression test results.

	ref_01			ref_03			FRMCom_02			FRMCom_03		
Cycle	Load (kN)	u_h (mm)	u_v (mm)	Load (kN)	u_h (mm)	u_v (mm)	Load (kN)	u_h (mm)	u_v (mm)	Load (kN)	u_h (mm)	u_v (mm)
1st	14.51	0.00	-0.02	26.15	0.02	-0.04	115.68	0.02	-0.07	82.83	0.01	-0.05
2nd	42.50	0.01	-0.06	54.79	0.03	-0.09	219.93	0.06	-0.15	198.38	0.03	-0.12
3th	72.47	0.03	-0.11	84.66	0.05	-0.14	339.56	0.22	-0.29	310.40	0.11	-0.23
4th	100.48	0.04	-0.16	110.27	0.07	-0.18	401.35	0.78	-0.53	386.43	0.76	-0.44
5th	115.88	0.06	-0.19	136.54	0.10	-0.24	418.32	1.41	-0.66	430.81	1.37	-0.71
6th	98.44	0.13	-0.28	146.17	0.24	-0.32	383.04	1.90	-0.79	394.21	1.63	-0.74
7th	80.36	0.38	-0.32	--	--	--	312.35	2.59	-0.75	315.35	2.48	-0.46
8th	50.89	1.33	-0.42	--	--	--	298.16	3.07	-1.02	--	--	--

The load vs displacement responses of the reference and strengthened specimens in terms of the averaged vertical and horizontal LVDT measurements are shown in Figure 6a) and Figure 6b). In general, the strengthened specimens have reached considerably higher strengths than the reference specimens. The post-peak behaviour of the reference specimens showed a smooth load decay, with the exception of specimen ref_03_cic, which was supposed to undergo a cyclic loading sequence but failed suddenly after reaching a considerably higher peak load than the remaining reference specimens. The responses registered for the strengthened specimens were, in general, similar, showing a pre-peak stage of significant load carrying capacity increase, and the peak load was reached for substantially higher displacements than the ones observed for the reference specimens. After peak load the strengthened specimens presented a relatively smooth load decay with the increase of the horizontal deformation.

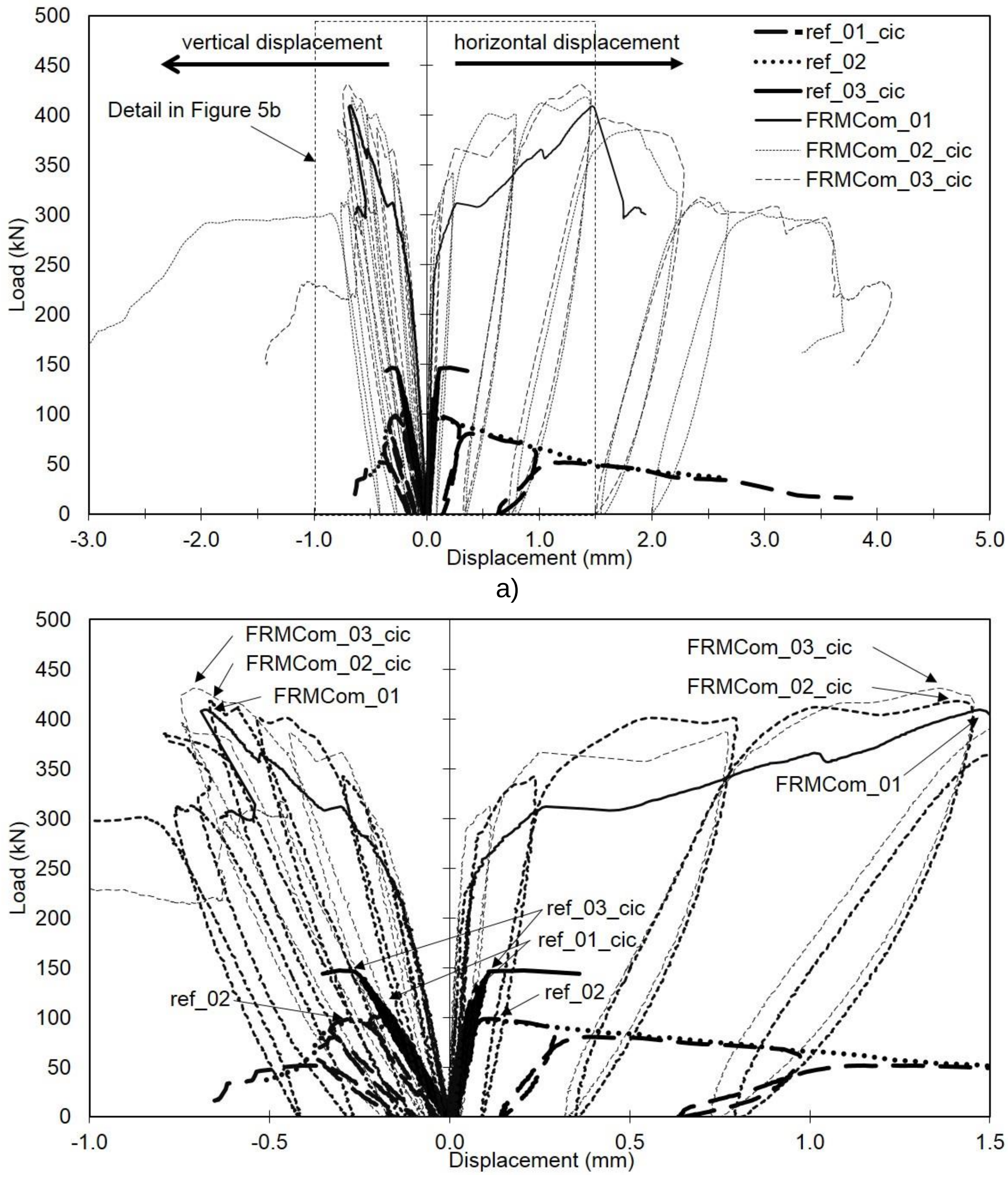

Figure 6 - Load vs displacement responses of the strengthened specimens: a) global response; b) detail of the response until peak.

The typical crack patterns observed at the surface of the reference and strengthened specimens after testing are presented in Figure 7a) and Figure 7b), respectively. The reference specimen presented a vertical crack that developed in a straight fashion from the lower to the upper support, very few and minor additional cracks presenting a very small tip opening developed after that main crack. The strengthened specimens presented, in a first phase, the same type of cracking as the reference specimens. However, at higher load levels multiple cracks developed and the failure was reached when the strengthening overlay started to detach from the masonry substrate (Figure 7c). This detachment occurred at the interface between the render layer (c in Figure 3) and the ceramic masonry brick surface, as shown in Figure 7c).

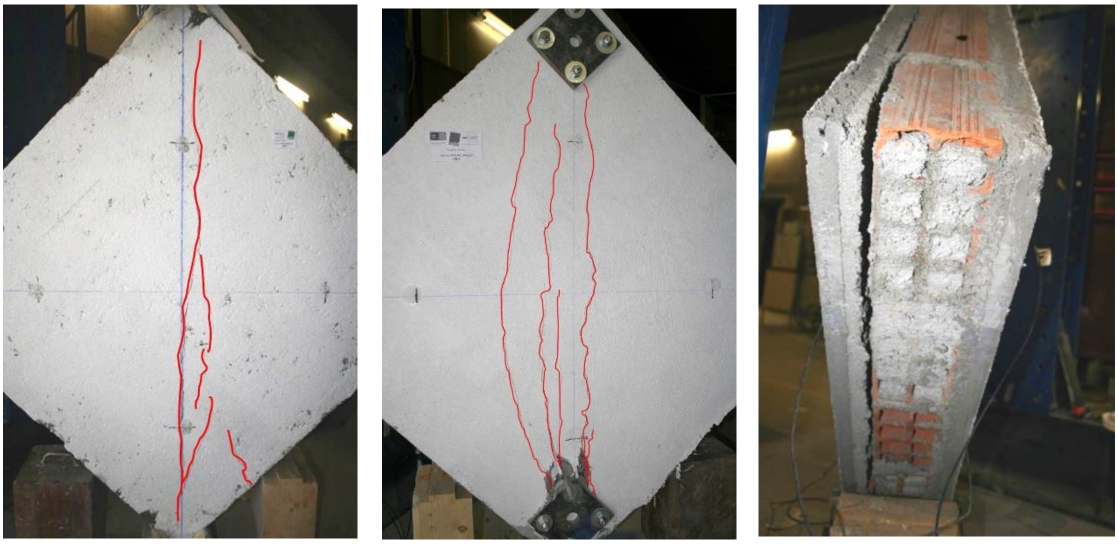

a) b) c)

Figure 7 - Image of the specimens after testing: a) Crack pattern in reference specimen, ref-02 side B; b) Crack pattern in strengthened specimen, FRMCom-03 side B; c) Detachment between the strengthening overlay and substrate, FRMCom-03.

5. DISCUSSION OF RESULTS

5.1. Peak values and capacity ratios

The responses presented in Figure 8 allow the clear distinguishing of the contribution of the strengthening system to the increase of the load carrying capacity of the tested masonry specimens. The shear stress and the shear strain were evaluated according to equation (1) and (3), respectively, where for *g* a value of 700 mm was considered. The shear strength of strengthened specimens was approximately two times higher than that of the reference walls. Considering the shear strain values obtained, the scatter of the results registered in the case of the reference specimens was greater, essentially due to the absence of the effect provided by the strengthening system for stabilising the fracture process. However, the strengthened specimens also showed a considerable scatter of results in terms of ultimate shear strain, in this case probably due to the influence of brittle failure modes such as the formation of the typical diagonal tensile crack and the detachment of the PFRM layers.

The maximum shear stress values obtained for cyclic testing were slightly higher than the values obtained in monotonic tests. This is explained by the possible accommodation of the loading shoes during the initial loading/ unloading cycles, providing a more homogeneous diagonal load transmission to the specimen and therefore a slight increase of load capacity.

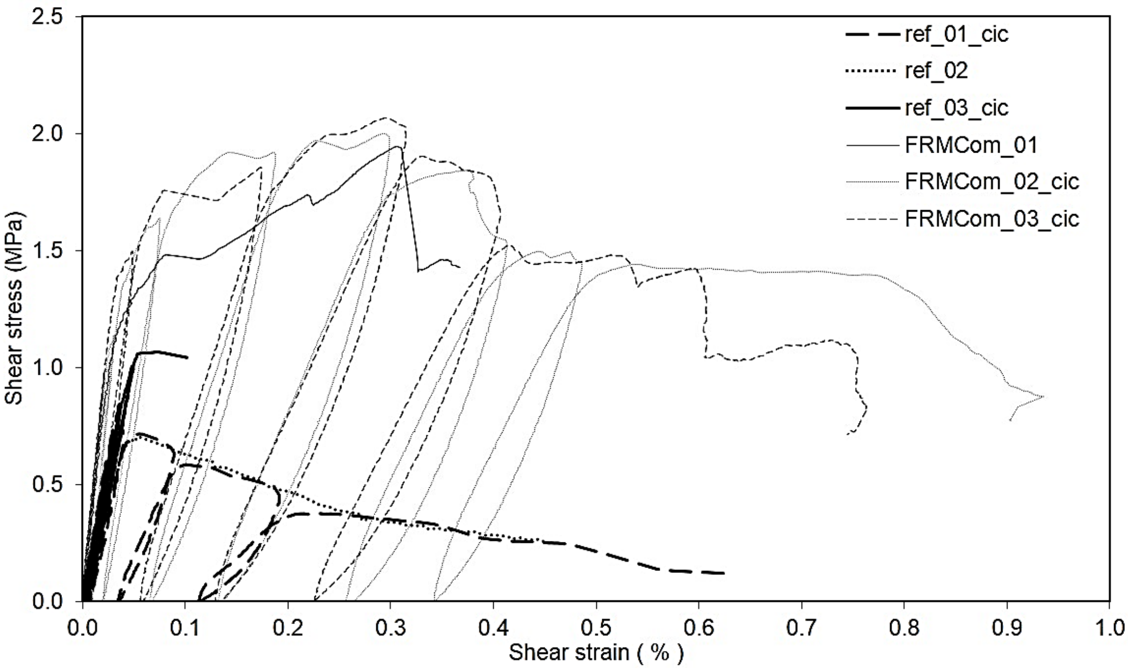

Figure 8 - Shear stress vs shear strain response of the specimens.

The collapse of the reference specimen ref_03_cic was reached shortly after the peak load was reached, as soon as the diagonal crack was formed. In contrast, the other two reference specimens have reached considerably higher deformation levels and the collapse took place after a gradual load decay. In general, all reference specimens have shown elastic responses almost up to the peak load. In contrast, the strengthened specimens exhibited a substantially increased post-cracking load carrying capacity. The non-linear portions of the responses were much more significant than in the case of the reference specimens. The energy dissipation capacity was assessed for the monotonic tests by computing the area under the load vs displacement response, where the displacement represented the distance difference between the two opposite loaded edges of the specimen during testing (see Figure 4). When comparing reference and strengthened panels the increment of 1390% of the dissipated energy was obtained. Considering that the monotonic load-displacement responses approximate well the envelope of the cyclic tests, similar results of the dissipated energy increments are expected for the cyclic tests.

The average values of the shear stress, the shear strain and the shear modulus are computed in Table 7 and 8. The ratios between the limit values of the shear stresses and the shear strains in the cases of the elastic and of the non-linear branches of the responses observed in the strengthened and in the reference specimens were computed as well. The elastic branch was considered to develop up to 33% of the peak load in the case of the specimens tested with monotonic loading, and up to the peak of the first cycle in the case of cyclic loading. These results show that the strengthening system has provided a shear strength increase of approximately 2.3.

Table 7– Average of the limit values of the shear stress, shearing strain and shear modulus obtained for the reference and the strengthened specimens.

Response range	Type of specimen	Shear Stress S_s (MPa)	Shearing Strain γ (%)	Modulus of shear stiffness G (MPa)
Elastic branch	Reference	0.185	0.007	2716.2
	Strengthened	0.532	0.012	4457.8
Peak	Reference	0.871	0.054	1696.1
	Strengthened	2.002	0.299	650.6

Table 8– Increase of capacity in terms of shear stress, shearing strain and increment of shear modulus obtained after strengthening.

Response range	Shear Stress S_s	Shearing Strain γ	Modulus of shear stiffness G
Elastic branch	2.1	1.1	1.6
Peak	2.3	5.5	0.4

The evolution of the damage due to the cyclic loading is shown in Table 9, where G_{cycle} represents the modulus of shear stiffness in each cycle, considering the linear part of the curve shear stress vs. shear strain during the loading sequence, and G_E represents the modulus of shear stiffness in the elastic branch of the first cycle. The specimens strengthened with the FRMCom system presented similar ratios G_{cycle}/G_E in the final cycles. In the case of the reference specimens the damage occurred suddenly in the case of the specimen ref_03, where the computed ratio was always 1.0 until failure. This result indicates that the specimen failed in a brittle manner. In the case of ref_01 the response obtained showed a gradual decay of the G_{cycle}/G_E ratio, in a similar fashion to the observed in the case of the strengthened specimens.

Table 9 – Variation of the Shear modulus during cyclic tests.

	ref_01		ref_03		FRMCom_02		FRMCom_03	
Cycle	G_{cycle} (MPa)	ratio G_{cycle}/G_E	G_{cycle} (MPa)	ratio G_{cycle}/G_E	G_{cycle} (MPa)	ratio G_{cycle}/G_E	G_{cycle} (MPa)	ratio G_{cycle}/G_E
Elastic	3326.6	--	2347.0	--	4427.2	--	4447.4	--
1st	3326.6	1.0	2347.0	1.0	4427.2	1.0	4447.4	1.0
2nd	2799.6	0.8	2297.7	1.0	4430.7	1.0	4467.3	1.0
3rd	2706.9	0.8	2358.8	1.0	4210.0	1.0	4513.1	1.0
4th	2526.8	0.8	2367.2	1.0	2627.8	0.6	3251.9	0.7
5th	2477.7	0.7	2436.7	1.0	1379.2	0.3	1325.5	0.3
6th	2083.7	0.6	2249.3	1.0	1044.5	0.2	975.7	0.2
7th	1036.0	0.3	--	--	913.9	0.2	847.3	0.2
8th	421.8	0.1	--	--	873.4	0.2	--	--

The effectiveness of different strengthening systems and the scatter of results obtained can be compared with the ones presented previously in Table 1. The mean values of the maximum load and coeficient of variation obtained in this research for reference specimens were 120 kN and 17%, which is expectable considering the brittle failure mechanism obtained. Meanwhile, for strengthened specimes the mean values of the maximum load and coeficient of variation obtained were 420 kN and 2%, representing a increase in the capacity of 250%. The number of specimens tested, although limited, agrees well with the number of specimens typically used by other authors for similar experimental characterizations and the coeficient of variation obtained is also comparable to the ones obtained by other researchers, as shown in Table 1.

5.1.1. Failure modes and crack patterns

During the diagonal tensile tests several types of mechanisms of structural degradation were observed (see Figure 9):

Type A. Crushing of the masonry units next to the supports, toe crushing, development of horizontal cracks, (ref_01, FRMCom_01).

Type B. Failure due to diagonal tensile stresses imposed during the tests, development of vertical cracks in the central area of the specimens (ref_01_cic, ref_02, ref_03_cic).

Type C. Delamination of the render and strengthening overlay from the masonry, development of vertical cracks between the masonry and the rendering layers. Delamination starts in the two free corners of the specimen (FRMCom_01, FRMCom_02_cic, FRMCom_03_cic).

Type D. Cracking and failure of webs and shells of the ceramic bricks (FRMCom_01, FRMCom_03_cic).

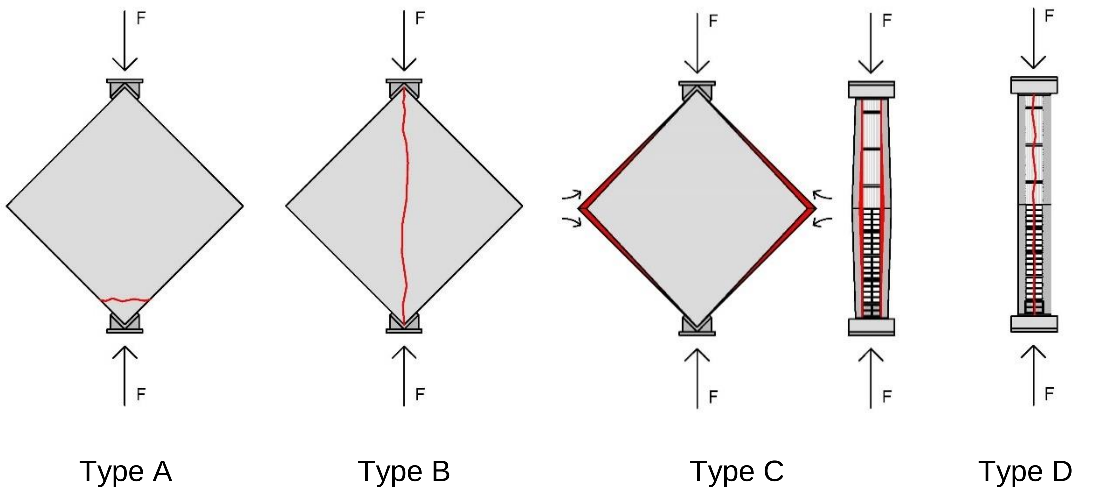

Figure 9 – Schematics of the different mechanisms leading to structural degradation during the diagonal tensile tests.

The failure of the specimens was reached after the development of one or more of these mechanisms. In the case of the reference specimens the mechanisms developed were mainly of the types B and D. In the case of strengthened specimens, a sequence of the mechanisms type B, C and D occurred before failure. The mechanism type A occurred only when the first strengthened specimen, FRMCom_01, was tested. In the subsequent tests this failure mode did not occur, since the hollows of the brick in this zone were filled with a high compressive strength mortar, and metallic plates were applied to provide additional confinement to the loading areas.

The instant at which the different mechanisms were initiated can be identified in the Figure 10, where the letters identify the stage at which the respective type of mechanism tends to occur. For both types of specimens, it was possible to trace the degradation of the stiffness of the load vs displacement response. The stiffness of the load vs horizontal displacement response is represented by the slope of the loading-unloading branches $K_{d,h}$, while the stiffness of the load vs vertical displacement response is represented by the slope of the loading-unloading branches, $K_{d,v}$. After the limit of the elastic branch was reached (point b in Figure 10), both slopes, $K_{d,h}$ and $K_{d,v}$, decrease faster for reference specimens, indicating that a higher degradation was obtained in each cycle. For the strengthened specimens the referred slopes show a lower variation per cycle, revealing that the contribution of the strengthening solution to the shear capacity of the specimens results in a reduction of the stiffness degradation. The variation of the stiffness of the load vs vertical displacement responses, $K_{d,h}$ and $K_{d,v}$, and of the ratios between the stiffness of the first and of the consecutive cycles are presented in Table 10.

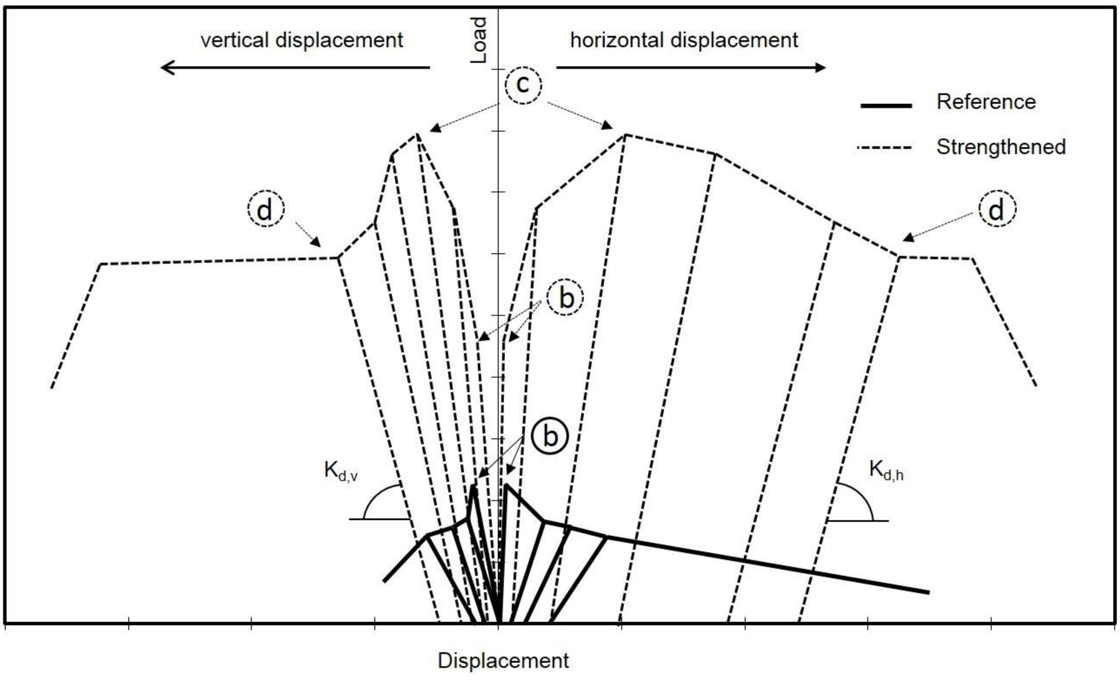

Figure 10 – Identification of the onset of the different types of damage mechanisms.

Table 10 – Evolution of the stiffness of the load vs horizontal displacement response from reference specimens under cyclic loading.

	ref_01				ref_03				FRMCom_02				FRMCom_03			
	K_{dv}	ratio	K_{dh}	ratio	K_{dv}	ratio	K_{dh}	ratio	K_{dv}	ratio	K_{dh}	ratio	K_{dv}	ratio	K_{dh}	ratio
Cycle	(kN/mm)	K_{dv}	(kN/mm)	K_{dh}	(kN/mm)	K_{dv}	(kN/mm)	K_{dh}	(kN/mm)	K_{dv}	(kN/mm)	K_{dh}	(kN/mm)	K_{dv}	(kN/mm)	K_{dh}
1st	-672	1.00	4266	1.00	-704	1.00	1714	1.00	-1671	1.00	6211	1.00	-1815	1.00	13252	1.00
2nd	-669	1.00	3118	0.73	-641	0.91	1876	1.09	-1620	0.97	5819	0.94	-1694	0.93	8146	0.61
3rd	-660	0.98	2787	0.65	-617	0.88	1841	1.07	-1431	0.86	3674	0.59	-1686	0.93	7242	0.55
4th	-637	0.95	2254	0.53	-615	0.87	1736	1.01	-1096	0.66	1261	0.20	-1353	0.75	2309	0.17
5th	-618	0.92	2081	0.49	-609	0.86	1605	0.94	-683	0.41	422	0.07	-816	0.45	439	0.03
6th	-413	0.62	1480	0.35	-555	0.79	1318	0.77	-557	0.33	229	0.04	-517	0.28	254	0.02
7th	-241	0.36	234	0.05					-426	0.26	120	0.02	-632	0.35	124	0.01
8th	-114	0.17	32	0.01					-345	0.21	98	0.02				

The crack patterns observed after the diagonal tensile tests are shown in Figure 11 and Figure 12. In general, the failure modes for the unreinforced masonry reference specimens were the typical ones expected for this type of test. In the case of the strengthened specimens the crack patterns observed, and failure mechanisms obtained, were influenced by the contribution of the strengthening system. The failure mode observed in this case was mostly characterized by a first phase where diagonal tensile cracks were developing, followed by the delamination of the render layer plus strengthening mortar, and a final stage of failure determined by the internal crushing of the units. In the case of the FRMCom_02 and FRMCom_03 specimens several cracks were formed, particularly next to the supports of the specimen, as shown in Figure 12. The onset of the damage mechanism type D (Figure 9) is clearly revealed by the sudden increase of the vertical displacement when compared to the horizontal ones (Figure 6), as identified in Figure 10 by the letter "d". The vertical displacement increments become, at this stage, much larger than the horizontal ones due to the crushing of the shells and webs of the ceramic bricks.

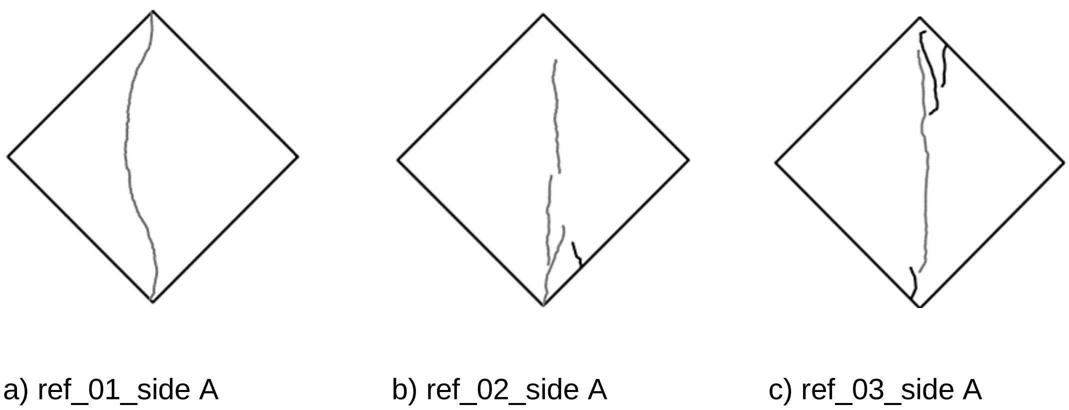

Figure 11 - Crack patterns of reference specimens after testing.

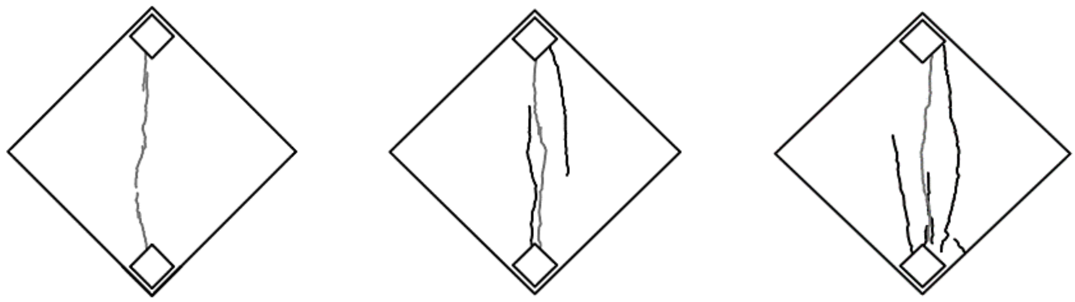

a) FRMCom_01_side A   b) FRMCom_02_side A   c) FRMCom_03_side A

Figure 12 - Crack patterns of strengthened specimens after testing.

5.2. Analytical description of the experimental results

According to the theory of elasticity, as previously discussed in the introductory section it can be assumed that during the diagonal tensile test the central area of a square masonry specimen is approximately subjected to a stress state where $\sigma_x = \sigma_y \cong -0.56P/A$ (compression) and $\tau_{xy} = 1.05P/A$. The principal stresses in this case are $\sigma_I \cong 0.5P/A$ and $\sigma_{II} \cong -1.62P/A$. The contribution of FRCM systems to the in-plane shear capacity can be calculated following the analytical methodology presented in ACI 549.4R-13, [33]. According to this standard the nominal shear capacity, V_n, is computed as shown in equation (5):

$$V_n = V_m + V_f \qquad (5)$$

where V_m represents the contribution of the masonry wall, and V_f represents the contribution of the FRM system.

The contribution of the masonry wall can be obtained according to the methodology presented by Li et al., [34], and applied to diagonal tensile tests by Babaeidarabad et al., [35]. Four types of failure mechanisms can occur, and the shear capacity for each type can be computed through the following equations:

- Shear capacity due to shear sliding failure, V_{ss}, calculated according to equation (6):

$$V_{ss} = \frac{\tau_0}{1 - \mu_0 \times tan\,\theta} \times A_n \qquad (6)$$

where τ_0 is the shear bond strength of the mortar joint (MPa), μ_0 is the coefficient of internal shear friction in mortar joints, θ is the angle between horizontal and main diagonal of the wall (degrees), and A_n is the net area of the cross section of the masonry wall (mm^2).

- Shear capacity due to shear friction failure, V_{sf}, calculated according to equation (7):

$$V_{sf} = \frac{\tau_{0,m}}{1 - \mu_m \times tan\,\theta} \times A_n \qquad (7a)$$

$$\tau_{0,m} = \frac{\tau_0}{1 + 1.5 \times \mu_0 \times \frac{h}{w}} \qquad (7b)$$

$$\mu_m = \frac{\mu_0}{1 + 1.5 \times \mu_0 \times \frac{h}{w}} \qquad (7c)$$

where $\tau_{0,\mathrm{m}}$ is the modified shear bond strength in mortar joint (MPa), with h and w being the height and length of the bricks (mm), respectively, and μ_m is the modified coefficient of internal shear friction in mortar joint.

- Shear capacity due to the diagonal tension failure, V_{dt}, calculated according to equation (8):

$$V_{dt} = \frac{tan\,\theta + \sqrt{21.16 + tan\,\theta^2}}{10.58} \times f'_t \times A_n \qquad (8)$$

where f'_t is the tensile strength of masonry, $f'_t = 0.67 \times \sqrt[2]{f'_m}$,(MPa), with f'_m being the compressive strength of the masonry (MPa)

- Shear capacity due to toe crushing failure at the loading end, V_c, calculated according to equation (9):

$$V_c = \frac{2 \times w \times f'_m}{3 \times h + 2 \times w \times tan\,\theta} \times A_m \qquad (9)$$

where A_m (mm^2) is de interface loading area between the steel shoe and the wall.

Finally the shear capacity of the unreinforced or plain wall, V_m, is the minimum value of previous expressions, see equation (10):

$$V_m = min\{V_{ss}; V_{sf}; V_{dt}; V_c\} \tag{10}$$

The behaviour of a near surface mounted FRP bars (NSM) based strengthening system is presented by Li et al., [34]. The developed theoretical formulation takes into account two different mechanisms, which are the debonding of the bar and the failure of the bar due to the tensile stresses. In contrast the FRMCom system uses a carbon mesh layer to resist the tensile stresses, and in this case only the failure of the fibres by tensile stresses is considered. The contribution of the FRM system for the shear capacity, V_f, is obtained according to equation (11):

$$V_f = 2 \times n \times A_f \times L \times f_{fv} \tag{11}$$

where n is the number of fabric layers, A_f is the area of mesh reinforcement by unit width (mm^2/mm), L is the length of the wall in the direction of the shear force (mm), f_{fv} is the design tensile strength of FRM shear reinforcement, $f_{fv} = E_f \times \varepsilon_{fv}$, (MPa), E_f is the tensile modulus of elasticity of the cracked FRM specimen, (MPa), and ε_{fv} is the design tensile strain of FRM shear reinforcement (mm/mm).

The shear capacity of the masonry specimens was calculated according to the analytical model presented previously using the values from Table 11. The compressive strength of the masonry was estimated according to EC6, since it was not possible to assess these parameters experimentally. However, previous studies conducted by Pereira et. al [36] indicate that these estimations, although slightly conservative, approximate well the experimental results. The characterization of the initial shear strength and the shear friction angle of mortar joints was carried by Capozucca [36], the values obtained are used in the analytical model as a lower bound value. The tensile behaviour of the FRCM composite system utilized was not experimentally characterized at this stage, since the failure is expected to be governed by the failure of the fibre mesh reinforcement. The mechanical characteristics of the FRCM system single components (matrix and fibre mesh) were previously presented in Table 3 and 4.

Table 11 – Values used in the analytical model to obtain the shear capacity of the specimens.

Description:	Value
Shear bond strength of the mortar joint, according to Capouzzuca [37]	$\tau_0 = 0.31$ MPa
Coefficient of internal shear friction in mortar joint according to Capouzzuca [37]	$\mu_0 = 0.60$
Angle between horizontal and main diagonal of the wall	$\theta = 45$ º
Net area of the masonry wall cross section	$A_n = 116600$ mm^2
Height of the brick units	$h = 195$ mm
Length of brick units	$w = 285$ mm
Compressive strength of the masonry (according to EC6 [13])	$f'_m = 1.14$ MPa
Interface loading area between the steel shoe and the wall specimen	$A_m = 33440$mm^2
Number of fabric layers	$n = 2$
Area of mesh reinforcement by unit width, CFM [32]	$A_f = 0.044$ mm^2
Tensile modulus of elasticity of the cracked FRM specimen [32]	$E_f = 240000$ MPa
Design value of the tensile strain of FRM reinforcement (according to ACI 549.R-13 [33])	$\varepsilon_{fv} = 0.004$ mm/mm
Ultimate tensile strain of FRM reinforcement according to the supplier [32]	$\varepsilon_{fv,ult} = 0.0175$ mm/mm
Tensile strength of the render mortar	$f_{t,r} = 2.11$ MPa
Net area of the render cross section	$A_{n,r} = 31800$ mm^2
Tensile strength of the PFRM	$f_{t,Ac} = 3.27$ MPa
Net area of the PFRM cross section	$A_{n,Ac} = 53000$ mm^2

The contribution of the rendering and PFRM layers, considering diagonal tensile failure, V_r and V_{PFRM}, are obtained according to equation (8) by using the net area of the cross section and the tensile strength of the respective materials.

Considering the equations (6) to (10) the result is a shear capacity of the unreinforced masonry wall, $V_m = 33.2\ kN$, and of the rendering layers, $V_r = 33.8\ kN$, which have to be summed in order to obtain the total capacity of the masonry specimen before strengthening, $V_{ref} = 67.0\ kN$.

With regards to the capacity of the strengthening system, according ACI 549.4R-13 the maximum allowable extension of the fibre reinforcement is 0.004 mm/mm. Considering this value and the equation (11), the maximum shear capacity of the strengthening system is $V_f = 118.3\ kN$. On the other hand, when considering the ultimate extension of the reinforcing fibres provided by the supplier, $\varepsilon_{fv,ult} = 0.0175$ mm/mm, [32], the maximum shear capacity is $V_{f,ult} = 517.5\ kN$. Finally, considering the diagonal tensile failure according to equation (8), the shear capacity of the PFRM layers is $V_{PFRM} = 87.3\ kN$.

The shear capacity values obtained experimentally are compared to the ones determined analytically in Table 10. Different experimental/analytical shear capacity ratios were computed, by following different sets of assumptions. For the reference case, the maximum shear capacity was estimated considering the contribution of the masonry, V_m, and rendering layer, V_r. For the "ACI" case, following ACI 549.4R-13, [33], the maximum shear capacity, V_{ACI}, was estimated considering the contribution of the masonry, V_m, of the rendering layer, V_r, and of the carbon strengthening mesh, V_f, by assuming 0.004 for the maximum allowable extension of the carbon fibres, as prescribed by ACI 549.4R-13, [33]. For the "ACI+PFRM" case, the maximum shear capacity, $V_{ACI+PFRM}$, was estimated considering the contribution of all previous factors and the additional contribution of the PFRM layers, V_{PFRM}. Finally for the "Sup" case, V_{Sup}, it was consider the contribution of all the elements and the maximum allowable extension of the carbon fibres prescribed by the supplier, $V_{f,ult}$.

While comparing the results obtained analytically to the experimental ones, see Table 12, it is possible to confirm that the procedure proposed by ACI 549.4R-13, [33], leads to conservative results. This procedure leads to a safety factor of 2.3, which may be considered somewhat high considering the low scatter of the experimental results obtained. This value compares with a safety factor of 1.33 proposed by ACI 549.4R-13, [33] for similar types of strengthening systems. However one may consider that the strengthening technique is still, to a certain extent, novel and therefore still encompasses significant uncertainties, most regarding durability and time dependent behaviour. When the contribution of the layers of the strengthening overlay is added to the analytical estimation, $V_{ACI+PFRM}$, the experimental vs analytical ratio decreases to 1.5. On the other hand, it is also possible to observe that, when considering the ultimate extension of the fibres, V_{Sup}^{an}, a ratio of 0.6 is obtained, meaning that the failure of the masonry model occurred before the ultimate extension in the fibres was reached. This was confirmed during the experimental program, since the failure was determined by the delamination of the strengthening system and crushing of the masonry, and not by the failure of the carbon mesh. Finally, if the contribution of the analytically estimated values of V_m and V_r is replaced by the experimentally obtained mean value of the diagonal tensile strength results in the reference specimens, the safety factors 1.8, 1.3 and 0.6 are obtained for V_{ACI}^{an} , $V_{ACI+PFRM}^{an}$ and V_{Sup}^{an}.

Table 12 – Shear capacity obtained for reference and strengthened specimens.

		Reference	Strengthened		
Experimental (kN)		V_{ref}^{exp} 119.8	V_{str}^{exp} 419.5		
Analytical		V_{ref}^{an}	V_{ACI}^{an}	$V_{ACI+PFRM}^{an}$	V_{Sup}^{an}
(kN)	$V_m = 33.2$	+	+	+	+
	$V_r = 33.8$	+	+	+	+
	$V_f = 118.3$	--	+	+	--
	$V_{f,ult} = 517.5$	--	--	--	+
	$V_{PFRM} = 87.3$	--	--	+	+
		67.0	185.3	272.6	671.8
	Ratio: Experimental/Analytical	1.8	2.3	1.5	0.6

6. CONCLUSIONS

The potentialities of a commercial system formed by a mortar reinforced with carbon fibre mesh (FRMCom system) for the strengthening of masonry walls were assessed in the present work by carrying out in-plane diagonal tensile tests. This strengthening system provided an increase of about 2.3 times of the shear strength of the reference specimens. The test procedure adopted allowed to evaluate the evolution of the damage in the specimens while subjected to cyclic loading, which was in general similar for all strengthened specimens. In the case of reference specimens, the damage developed in a more sudden manner.

In general, the failure modes of the reference specimens were the typical ones and expected for diagonal tensile testing. In contrast, the failure modes and crack patterns obtained for the strengthened specimens were characterized by a first phase at which the normal diagonal tensile cracks were developing gradually, followed by the delamination of the strengthening mortar immediately before failure. Additionally, in the case of the strengthened specimens several cracks were formed, particularly next to the supports of the specimen.

The adoption of a cyclic loading procedure on the diagonal tensile test, for the experimental characterization of the masonry, allowed the assessment of the stiffness degradation during each cycle, as well as the deterioration of the strengthening mechanisms. Additionally, it was possible to verify the adequacy of this test to assess the relevant in-plane failure mechanisms for typical masonry walls.

Although the experimental programme was limited the dispersion of the results allowed to assess and quantify the contribution by the strengthening system to the increase of the load carrying capacity with a reasonable accuracy. The FRMCom system strengthening technique provided a significant increment of strength and energy dissipation ability to this type of construction system, as well as higher shear strain combined with lower scatter of the obtained results. The delamination of the strengthening overlay may suggest that, in some cases, the adoption of transverse connecting systems between the masonry opposite faces may become essential to fully explore the contribution of the strengthening overlay to the load carrying capacity increment.

The analytical model described by ACI 549.4R-13 led to results that can be considered conservative, with a safety factor of 2.3. This is in part explained by the neglecting of the contribution of the layers of the strengthening mortar and by the limitation of the tensile strain of the carbon fibres to a value of 0.004 mm/mm. When the contribution of the strengthening mortar is considered, the safety factor decreases to 1.5. Finally, when the carbon fibres are allowed to reach the ultimate tensile strain of 0.0175 mm/mm, a safety factor of 0.6 is obtained indicating the premature failure of the strengthening system. This result was corroborated by the experimental results, where the premature failure of the strengthened specimens was observed before the ultimate tensile strain was reached on the carbon fibre reinforcement.

Acknowledgements

This research was carried in the framework of InoTec, Innovative material of ultra-high ductility for the rehabilitation of the built patrimony, funded by COMPETE/QREN/FEDER (NORTE-07-0202-FEDER-023024). InoTec project is promoted by CiviTest company and University of Minho. S&P Clever Reinforcement Ibérica is gratefully acknowledged for providing the materials used in the strengthening of the masonry specimens.

References

[1] M. A. Elgawady, P. Lestuzzi, and M. Badoux, “A review of conventional seismic retrofitting techniques for URM,” in *13th International Brick and Block Masonry Conference*, 2004, pp. 1–10.

[2] S. B. Kadam, Y. Singh, and B. Li, “Strengthening of unreinforced masonry using welded wire mesh and micro-concrete – Behaviour under in-plane action,” *Constr. Build. Mater.*, vol. 54, pp. 247–257, 2014.

[3] A. Figueiredo, H. Varum, A. Costa, D. Silveira, and C. Oliveira, “Seismic retrofitting solution of an adobe masonry wall,” *Mater. Struct.*, vol. 46, no. 1–2, pp. 203–219, Jul. 2012.

[4] C. G. Papanicolaou, T. C. Triantafillou, K. Karlos, and M. Papathanasiou, “Textile-reinforced mortar (TRM) versus FRP as strengthening material of URM walls : in-plane cyclic loading,” *Mater. Struct.*, vol. 40, pp. 1081–1097, 2007.

[5] E. Bernat-Maso, C. Escrig, C. A. Aranha, and L. Gil, “Experimental assessment of Textile Reinforced Sprayed Mortar strengthening system for brickwork wallettes,” *Constr. Build. Mater.*, vol. 50, pp. 226–236, 2014.

[6] M. Corradi, A. Borri, G. Castori, and R. Sisti, “Shear strengthening of wall panels through jacketing with cement mortar reinforced by GFRP grids,” *Compos. Part B Eng.*, vol. 64, pp. 33–42, 2014.

[7] Federal Emergency Management Agency, *Techniques for the Seismic Rehabilitation of Existing Buildings - FEMA 547*. Books Express Publishing, 2006, p. 572.

[8] Y. Kim, H. Kong, and V. C. Li, “Design of engineered cementitious composite suitable for wet-mixture shotcreting,” *ACI Mater. J.*, no. 100, 2003.

[9] E. Esmaeeli, E. Manning, and J. A. O. Barros, “Strain hardening fibre reinforced cement composites for the flexural strengthening of masonry elements of ancient structures,” *Constr. Build. Mater.*, vol. 38, pp. 1010–1021, Jan. 2013.

[10] A. Dehghani, G. Fischer, and F. Alahi, “Strengthening masonry infill panels using engineered cementitious composites,” *Mater. Struct.*, 2013.

[11] M. A. Elgawady, P. Lestuzzi, and M. Badoux, “Retrofitting of masonry walls using shotcrete,” in *2006 NZSEE Conference, Yeni Zelanda*, 2006, no. 45.

[12] American Society for Testing and Materials, *E 519-02 Standard test method for diagonal tension (shear) in masonry assemblages*. 2002, pp. 1–5.

[13] Comité Européen de Normalisation, “EN 1996-1-1:1995 Eurocode 6 - Design of masonry structures - Part 1-1: General rules for reinforced and unreinforced masonry structures.” Comité Européen de Normalisation, Brussels, CEN members, pp. 1–123, 2005.

[14] B. Silva, M. Dalla Benetta, F. da Porto, and C. Modena, “Experimental assessment of in-plane behaviour of three-leaf stone masonry walls,” *Constr. Build. Mater.*, vol. 53, pp. 149–161, Feb. 2014.

[15] J. Milosevic, A. S. Gago, M. Lopes, and R. Bento, “Experimental assessment of shear strength parameters on rubble stone masonry specimens,” *Constr. Build. Mater.*, vol. 47, pp. 1372–1380, Oct. 2013.

[16] A. Brignola, S. Frumento, S. Lagomarsino, and S. Podestà, “Identification of Shear Parameters of Masonry Panels Through the In-Situ Diagonal Compression Test,” *Int. J. Archit. Herit.*, vol. 3, no. 1, pp. 52–73, Dec. 2008.

[17] A. Borri, G. Castori, M. Corradi, and E. Speranzini, “Shear behavior of unreinforced and reinforced masonry panels subjected to in situ diagonal compression tests,” *Constr. Build. Mater.*, vol. 25, no. 12, pp. 4403–4414, Dec. 2011.

[18] F. Parisi, I. Iovinella, A. Balsamo, N. Augenti, and A. Prota, “In-plane behaviour of tuff masonry strengthened with inorganic matrix – grid composites,” *Compos. Part B*, vol. 45, no. 1, pp. 1657–1666, 2013.

[19] N. Ismail, R. B. Petersen, M. J. Masia, and J. M. Ingham, “Diagonal shear behaviour of unreinforced masonry wallettes strengthened using twisted steel bars,” *Constr. Build. Mater.*, vol. 25, no. 12, pp. 4386–4393, Dec. 2011.

[20] A. Borri, G. Castori, and M. Corradi, “Shear behavior of masonry panels strengthened by high strength steel cords,” *Constr. Build. Mater.*, vol. 25, no. 2, pp. 494–503, Feb. 2011.

[21] J. A. P. P. de Almeida, E. N. B. Pereira, and J. A. O. Barros, “Performance assessment of overlay strengthened masonry under cyclic loading using the diagonal tensile test,” in *9th International Masonry Conference, July 7, 8, 9; Guimarães*, 2014.

[22] H. Santa-Maria, G. Duarte, and A. Garib, “Experimental Investigation of masonry panels externally strengthened with CFRPlaminates and fabric subjected to in-plane shear load,” in *13th World Conference on Earthquake Engineering*, 2004, no. 1627, pp. 1–10.

[23] F. F. S. Pinho, V. J. G. Lúcio, and M. F. C. Baião, “Rubble stone masonry walls in Portugal strengthened with reinforced micro-concrete layers,” *Bull. Earthq. Eng.*, vol. 10, no. 1, pp. 161–180, Apr. 2011.

[24] G. F. M. Vasconcelos and P. B. Lourenço, “Experimental characterization of stone masonry in shear and compression,” *Constr. Build. Mater.*, vol. 23, no. 11, pp. 3337–3345, Nov. 2009.

[25] A. Gabor, A. Bennani, E. Jacquelin, and F. Lebon, “Modelling approaches of the in-plane shear behaviour of unreinforced and FRP strengthened masonry panels,” *Compos. Struct.*, vol. 74, pp. 277–288, 2006.

[26] B. Ozsayin, E. Yilmaz, M. Ispir, H. Ozkaynak, E. Yuksel, and A. Ilki, “Characteristics of CFRP retrofitted hollow brick infill walls of reinforced concrete frames,” *Constr. Build. Mater.*, vol. 25, no. 10, pp. 4017–4024, 2011.

[27] C. Calderini, S. Cattari, and S. Lagomarsino, “The use of the diagonal compression test to identify the shear mechanical parameters of masonry,” *Constr. Build. Mater.*, vol. 24, no. 5, pp. 677–685, 2010.

[28] M. Frocht, “Recent advances in photoelasticity,” *ASME Trans*, vol. 55, no. September–December, pp. 135–53, 1931.

[29] Comité Européen de Normalisation, “EN 772-1:2000 Methods of test for masonry units. Determination of compressive strength.” Comité Européen de Normalisation, Brussels, p. 14, 2000.

[30] Comité Européen de Normalisation, “EN 1015-11:1999 Methods of test mortar for masonry – Part 11: Determination of flexural and compressive strength of hardened mortar.” Brussels, 1999.

[31] Comité Européen de Normalisation, “EN 1015-12:2000 Methods of test for mortar for masonry - Part 12: Determination of adhesive strength of hardened mortar.” Brussels, 2000.

[32] S&P Clever Reinforcement Company AG, “S&P ARMO-System FRCM Design Guidelines - Fiber Reinforced Cementitious Matrix (VER12.03.2013/IND),” Seween, 2013.

[33] American Concrete Institute (ACI), “ACI 549.4R-13 Guide to Design and Construction of Externally Bonded Fabric- Reinforced Cementitious Matrix (FRCM) Systems for Repair and Strengthening Concrete and Masonry Structures.” Farmington Hills, Michigan, 2014.

[34] T. Li, N. Galati, J. G. Tumialan, and A. Nanni, “Analysis of unreinforced masonry concrete walls strengthened with glass fiber-reinforced polymer bars,” *ACI Struct. J.*, vol. 102, no. 4, 2005.

[35] S. Babaeidarabad, D. Arboleda, G. Loreto, and A. Nanni, “Shear strengthening of un-reinforced concrete masonry walls with fabric-reinforced-cementitious-matrix,” *Constr. Build. Mater.*, vol. 65, pp. 243–253, 2014.

[36] P. M. F. Pereira, J. B. Aguiar, A. Camões, and P. B. Lourenço, “The Portuguese masonry’s mechanical characterization,” in *8th International Masonry Conference 2010 in Dresden*, 2010, pp. 611–622.

[37] R. Capozucca, “Shear Behaviour of Historic Masonry Made of Clay Bricks,” *Open Constr. Build. Technol. J.*, vol. 5, no. suppl 1M6, pp. 89–96, 2011.